Available online at www.sciencedirect.com
SCIENCE DIRECT®
Journal of Sound and Vibration 281 (2005) 743–762
JOURNAL OF SOUND AND VIBRATION
www.elsevier.com/locate/jsvi

Piezoelectric sensors and actuators for milling tool stability lobes

Neil D. Sims[a,*,1], Phillip V. Bayly[b], Keith A. Young[c]

[a]*Department of Mechanical Engineering, The University of Sheffield, Mappin Street, Sheffield S1 3JD, UK*
[b]*Washington University, Campus Box 1185, One Brookings Drive, St Louis, MO 63130-4899, USA*
[c]*The Boeing Company, P.O. Box 516, St Louis, MO, USA*

Received 15 May 2003; accepted 2 February 2004
Available online 14 October 2004

Abstract

In this article, the authors describe the use of piezoelectric sensors and actuators for the prediction of milling tool stability lobes, since existing methods for predicting tool stability have disadvantages which limit their practical use. An experimental approach is described whereby modal testing is performed using surface-mounted piezoelectric sensors and actuators to generate a prediction of tool instability due to regenerative chatter. The approach is first demonstrated by synthetic modal analysis based upon a finite element model of a cantilever beam. Laboratory tests are then performed on small milling tools, and it is shown that there is good agreement with alternative methods for predicting stability. It is concluded that the proposed technique may be more readily suited to automation, and is more appropriate for use on very small milling tools.

1. Introduction

High-speed machining is a potentially unstable system, where the forces generated by the cutting process are coupled to the dynamic behaviour (stiffness, damping, and inertia) of the

*Corresponding author. Tel: +44-114-2227724; fax: +44-114-2227890.
E-mail address: n.sims@sheffield.ac.uk (N.D. Sims).
[1]working in association with the Advanced Manufacturing Research Centre with the Boeing Company, www.amrc.co.uk.

0022-460X/$ - see front matter © 2004 Elsevier Ltd. All rights reserved.
doi:10.1016/j.jsv.2004.02.014

Nomenclature

b	depth of cut
b_b	breadth of a beam
$b_{\lim}$	depth of cut at the limit of stability
b_p	breadth of a piezoelectric transducer
C_p	capacitance of a piezoelectric transducer
D_3	electric displacement of a piezoelectric transducer
d_{31}	piezoelectric constant
$E_{0,12}$	static correction for a modal model, α_{12}, based upon truncated modes
E_3	electric field
F	cutting force
f_t	actuation force the tip of the tool
G_{OTF}	orientated transfer function, $Y(\omega)/F(\omega)$
h	chip thickness
H_{12}	receptance frequency response function, measured at location $_1$ due to actuation at $_2$
h_m	mean chip thickness
k_a	piezoelectric actuator gain
K_s	cutting stiffness
k_s	piezoelectric sensor gain
m	number of teeth on the milling tool
M_a	bending moment induced by a piezoelectric actuator
M	number of modes in the truncated modal model
N	number of complete surface waves between subsequent tooth passes
n	mode number (mode of vibration)
$_nA_{12}$	modal constant for mode n and measurement H_{12}
N_{ct}	number of cutting teeth
S_1	strain
t	time
t_b	thickness of a beam
T_1	stress
t_b	beam thickness
t_p	piezoelectric transducer thickness
v_a	piezoelectric actuator voltage
v_s	piezoelectric sensor voltage
x_t	tool displacement at the tip
x	coordinate along the neutral axis of a beam
Y	tool vibration
y	coordinate normal to the neutral axis of a beam
Y_0	tool vibration for the previous tool pass
Y_p	young's modulus
α_{tt}	frequency response prediction based upon a modal model with a static correction term
α_{tt}^P	frequency response prediction based upon a modal model with no static correction term
α	angle between Y and F
ε	phase between surface waves on workpiece
ε_{33}	permittivity of piezoelectric material
ϕ_{1n}	mode shape for mode $_n$ at location $_1$
ω	vibration frequency
Ω	rotation frequency of the spindle

machine structure, tool, and workpiece. A common form of instability during machining, known as regenerative chatter, is due to the generation of surface waviness which modulates the cutting force. In the case of single-point orthogonal cutting operations (eg turning), this process was modelled by Tlusty [1] over 40 years ago. In the case of milling operations, the same theory can be used to indicate approximate stability conditions, and the technology is now available commercially for machine-shop use [2].

In many cases, the workpiece is essentially rigid in comparison with the tool, and so the prediction of chatter requires a measurement of the driving-point frequency response function (FRF) of the tool at the cutting surface. This measurement is currently made with a modal

hammer and collocated accelerometer, while the tool is mounted on the spindle. Whilst this approach yields good predictions of chatter stability, there are a number of potential problems. For example, the modal test requires a skilled (or trained at the very least) user in order to perform the test, validate the data, and interpret the stability prediction. The test process itself requires periods of machine down time, which may interfere with the production schedule, and repeatability of the test data is not guaranteed between machine set-ups. Finally, frequency response generation with a modal hammer is not effective on very small tools, where it becomes impossible to accurately strike the tool tip.

In an effort to resolve these issues, some alternative approaches to the chatter prediction problem have been proposed. For example, researchers have suggested a receptance coupling method to enable tool testing to be performed off the machine [3]. However, repeatability issues cannot be addressed, and an expert user is again required. Another approach is to predict the tool FRF using finite element software [4], but errors in the model's damping and stiffness matrix lead to inaccurate predictions, so the approach is really only useful for tool specification. To avoid the requirement for a tool FRF measurement, audio-processing techniques have been developed to identify stable spindle speeds from a sound measurement during cutting [5,6]. However, stable depths of cut cannot be predicted, and skilled users are required. Recently, a stable speed test apparatus has been proposed [7], but again this is unable to predict stable depths of cut.

One potentially attractive approach to obtaining the tool tip frequency response data is to excite the tool with a surface-bonded piezoelectric actuator. Compared to a modal hammer, this approach offers more control over the excitation signal, thus reducing the effects of signal noise. The approach is more amenable to automation which avoids user error, reduces tool downtime, and enables more regular testing to reduce repeatability problems. Finally, the method is more suitable for miniature tools. However, a disadvantage is that the tool tip FRF cannot be measured directly and so some modal analysis or signal-processing steps are required. The piezoelectric material must also be mounted onto the tool structure, and the electrical connections made. These can be rather delicate operations, but in the future it may be possible to manufacture tools with embedded piezoelectric transducers.

In this work, the authors describe an experimental procedure that has been used to predict tool stability using piezoelectric transducers. In Section 2, the background theory is drawn together to demonstrate how tool stability could be predicted from the experimental data. In Section 3 a numerical study is described which demonstrates the concept, and in Section 4 a milling tool is tested in the laboratory. Following a discussion of the results, some conclusions are drawn on the performance of the proposed technique and its advantages compared to alternative methods.

2. A review of the theory

The theory of regenerative chatter is not necessarily well known within the field of vibration research, and so this section begins with a derivation for the stability condition for turning operations. This is followed by a brief discussion of the issues that arise during milling. For a more detailed discussion, the interested reader is referred to ref. [8,9].

2.1. Stability lobes

2.1.1. Turning

In Fig. 1, a cutting tooth is removing a chip of material from the workpiece, which is moving toward the tool. The depth of cutting is b, and the chip thickness is h. The workpiece is assumed to be rigid, whilst the tool is flexible with a single mode of vibration normal to the cut surface as indicated. As usual, it is assumed [10] that the force F on the tool due to the cutting operation is related to the chip geometry by

$$F = K_s bh, \tag{1}$$

where K_s is known as the cutting stiffness that relates the depth of cut to the resulting force.

After one rotation of the workpiece, the tool cuts into the surface produced by the cutter at the previous rotation, or 'pass'. The chip thickness is therefore given by

$$h = h_m + Y_0 - Y. \tag{2}$$

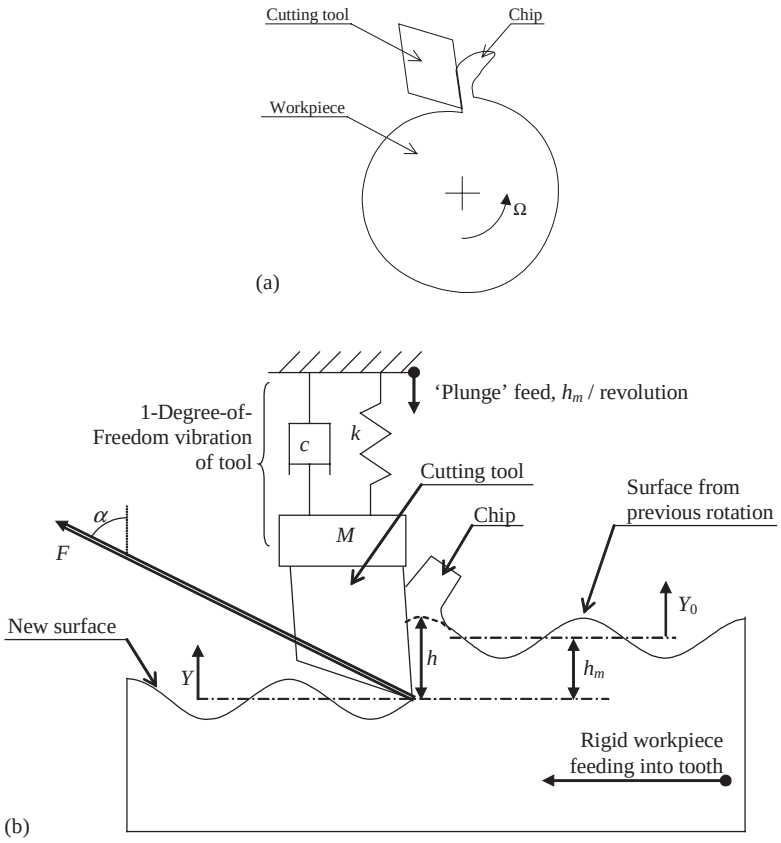

Fig. 1. Regenerative chatter in turning, for a single mode of vibration with stiffness k, damping c, and mass M. (a) Turning operation; (b) chatter mechanism for a single degree-of-freedom tool.

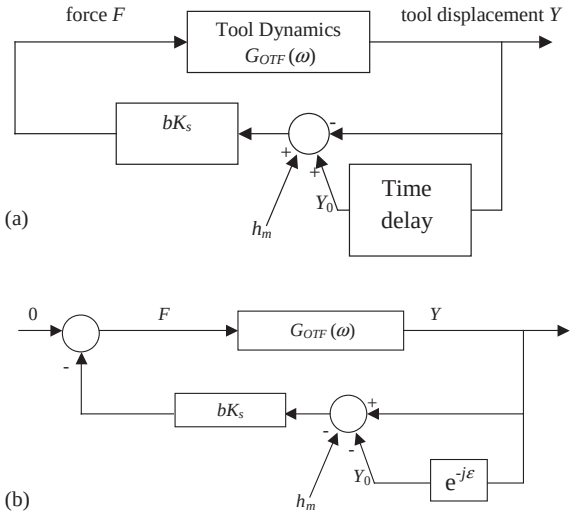

Fig. 2. Block diagram of the regenerative chatter mechanism. (a) Physical process; (b) rearranged as a negative feedback process.

With reference to Eq. (2) and Fig. 1b, h_m is the mean chip thickness due to the tool moving into the workpiece during the cutting operation. Y is the current vibration of the tool from its mean position, and Y_0 is the vibration from the mean position for the previous pass.

The cutting operation can therefore be described with the block diagram shown in Fig. 2a. Here, the *orientated transfer* function, G_{OTF}, between the cutting force F and the resulting vibration Y is given by

$$G_{\mathrm{OTF}}(w) = F\,\cos(a)\,G(w), \tag{3}$$

where $G(\omega)$ is the transfer function, or FRF, from a force applied in the direction of the mode of vibration and the resulting motion in that direction. The angle α is depicted in Fig. 1b. With reference to Fig. 2a, it is worth noting that the mechanism of regenerative chatter is based upon the inherent feedback of vibration (i.e. self-excited vibration due to the cutting stiffness), and not the changing frictional forces that arise during metal cutting, which are attributed to other less significant forms of chatter [11].

For a linear system, the vibrations Y and Y_0 will be sinusoidal with the same frequency but delayed by a phase ε. Redrawing the block diagram shown in Fig. 2a as a negative feedback process gives the block diagram shown in Fig. 2b. For stability analysis of a linear system, the constant value h_m can be neglected, and the Nyquist stability criterion can be applied to Fig. 2b, giving

$$K_s b_{\mathrm{lim}} G_{\mathrm{OTF}}(j\omega)\left(1 - \mathrm{e}^{-\mathrm{j}\varepsilon}\right) = -1, \tag{4}$$

where b_{lim} is the value of b at the point of stability. The vectors can be represented on the Nyquist plot, as shown in Fig. 3. Note that $\mathrm{e}^{-\mathrm{j}\varepsilon}$ is a unit vector, and K_s, and b_{lim} are real. This gives

$$b_{\mathrm{lim}} = \frac{-1}{2K_s \mathrm{Re}(G_{\mathrm{OTF}}(\mathrm{j}\omega))}, \tag{5}$$

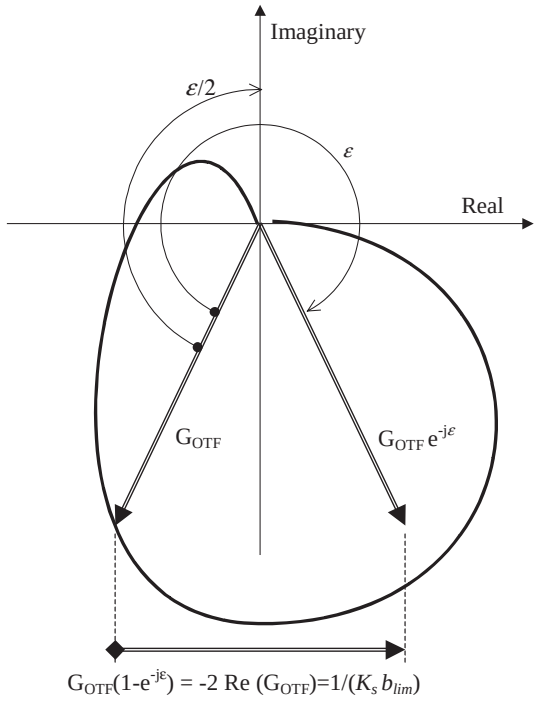

Fig. 3. Nyquist diagram for $G_{\mathrm{OTF}}(\omega)$, with Eq. (4) superimposed.

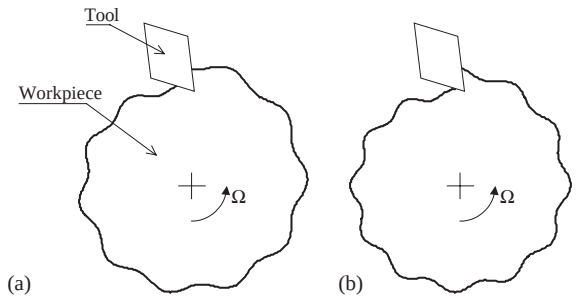

Fig. 4. Regenerative chatter in turning: surface waves. (a) 10.6 waves between tooth passes: $N = 6$; $\varepsilon = 0.6 \times 2 \times \pi$; (b) 12 waves between tooth passes: $N = 12$; $\varepsilon = 0 \times 2 \times \pi$.

which defines the limiting depth of cut, b_{lim}, for stable cutting at a given vibration frequency ω. The vibration frequency is related to the workpiece rotation speed Ω (in rad/s) by the formula

$$\Omega = \omega/(N + \varepsilon/2\pi), \quad N = 0, 1, 2, 3, \ldots, \tag{6}$$

where N is the largest possible integer such that $\varepsilon < 2\pi$. Eq. (6) defines the number of waves of vibration $(N + \varepsilon/2\pi)$ between consecutive passes of the tool, as illustrated in Fig. 4.

To summarise, the FRF for the tool, $G(\omega)$, can be scaled to give the so-called orientated transfer function $G_{\mathrm{OTF}}(\omega)$. Each frequency ω of the transfer function $G_{\mathrm{OTF}}(\omega)$ has a limiting

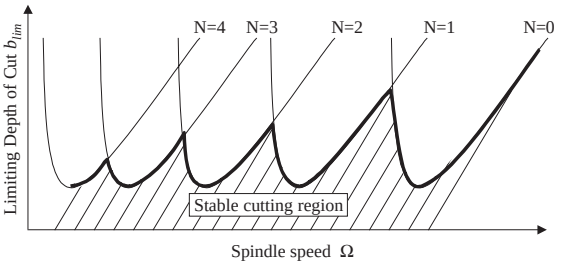

Fig. 5. Stability lobes diagram for a single degree-of-freedom structure.

depth of cut given by Eq. (5), a phase ε defined by Fig. 3, and a series of corresponding spindle speeds—one for each value of N—given by Eq. (6).

This results in the stability lobe diagram, which illustrates the relationship between stable depth of cut and spindle speed. For a single mode of vibration, a typical stability lobe is shown in Fig. 5.

The stability lobe diagram has enormous significance in practice: if the transfer function of the tool tip is known, then the cutting stability can be predicted for a range of spindle speeds.

2.1.2. Milling

The analysis of milling chatter is made considerably more complex, since the cutting tool is rotating rather than the workpiece, there is more than one cutting tool, and the cutting teeth are usually not straight (due to the flute helix of the tool), so that cutting is not orthogonal. The direction and magnitude of the cutting force will change as teeth engage and rotate in the workpiece. Consequently, many researchers have proposed time-domain solutions to predict chatter during milling [9,12], which usually rely on a modal model of the tool's dynamic behaviour at the cutting location (i.e. the tip of the tool). Alternatively, approximate solutions have been proposed which extend the analytical result to the case of milling. Two popular methods are that proposed by Altintas [13], and that used in the commercial software MetalMax TXF [14]. Here we use the approach described by Smith and Tlusty [10], which is also consistent with Ref. [14]. The cutting process is now shown schematically in Fig. 6, from which Eq. (6) can be rewritten as

$$N + \varepsilon/2\pi = \omega/(\Omega m), \tag{7}$$

where Ω is now the speed of rotation of the milling tool (in rad/s), and m is the number of teeth on the cutter. If one assumes that the cutting force F acts in the middle of the cutting sector, and is scaled by the average number of cutting teeth, then Eq. (5) can be rewritten as

$$b_{\lim} = \frac{-1}{N_{\mathrm{ct}} 2K_s \mathrm{Re}(G_{\mathrm{OTF}}(\mathrm{j}\omega))}, \tag{8}$$

where N_{ct} is the average number of cutting teeth, which is determined from the radial immersion of the tool into the workpiece, and the tool diameter.

In practice, the tool and spindle will have modes of vibration in mutually perpendicular directions, and all these modes will contribute to the orientated transfer function. The FRFs in the two directions are usually measured using a modal hammer and co-located accelerometer, and the frequency response integrated twice to give the receptance FRF.

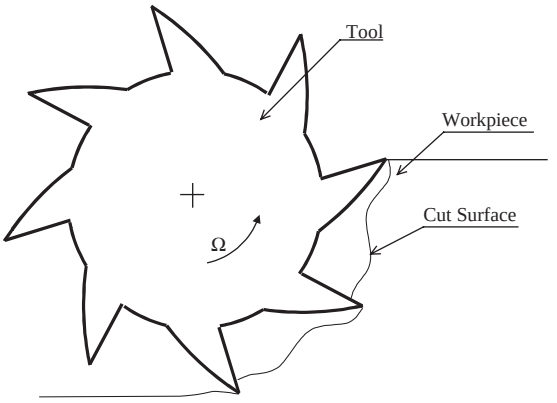

Fig. 6. Regenerative chatter mechanism in milling. In the case shown, there are eight teeth on the cutter ($m=8$) and approximately 1.6 surface waves between each tooth pass ($N=1;\ \varepsilon=0.6\times2\times\pi$).

For the approximate analytical solution summarised here, the FRFs are scaled (depending upon the cutting geometry) and summed to give the orientated transfer function (G_{OTF}). Only the negative real part of G_{OTF} will dictate stability.

For time-domain simulations of milling operations, the FRFs of the tool tip are usually used to create a modal models of the tool's vibration behaviour at the cutting location. These models will then be used within the time-domain simulation.

2.2. Modal analysis of piezostructures

To recap, the analysis of regenerative chatter during milling requires a knowledge of the driving-point (i.e. collocated) receptance FRFs at the tool tip. These measurements are currently obtained using a modal hammer and accelerometer, but this is not always practicable. The focus of the present contribution is to develop an alternative method of predicting these FRFs using piezo-actuators and sensors, and to illustrate the accuracy in terms of the stability lobe prediction. In this section, the relevant theory is drawn together to describe the approach.

2.2.1. Problem definition

Consider the milling spindle system shown schematically in Fig. 7a. The aim is to identify experimentally the FRF between the applied force F_t and the resulting deflection x_t—a task that is traditionally achieved using a modal hammer and accelerometer.

Fig. 7b illustrates the tool holder and tool in more detail. Two patches of piezoelectric material have been added near the root of the tool, one being excited by a voltage $v_a(t)$ and the other acting as a sensor and producing a voltage $v_s(t)$. The task is to reconstruct the FRF at the tool tip: $x_t(\omega)/f_t(\omega)$ (referred to as $G(\omega)$ in the preceding section), given the FRFs $v_s(\omega)/v_a(\omega)$ and $x_t(\omega)/v_a(\omega)$. Actuation at the tool tip is no longer necessary, and although the measurement x_t is still required, this can be achieved with a non-contacting sensor such as a laser doppler vibrometer.

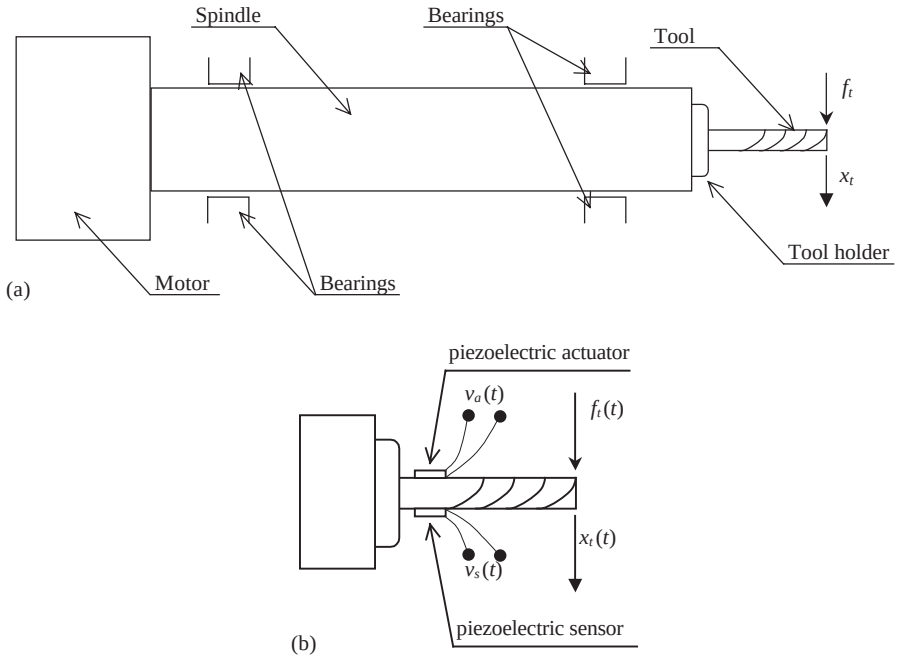

Fig. 7. Milling tool and spindle schematic. (a) General arrangement; (b) close-up of the tool with a surface-mounted piezoelectric sensor and actuator.

2.2.2. *Piezostructures*

The constitutive laws for a piezoelectric material can be written as a coupled electromechanical problem in a form similar to thermoelastic problems [15,16]. Dosch et al. [17] noted that the general constitutive equations are underdetermined, but that the following scalar case is often valid:

$$\begin{aligned} S_1 &= \frac{1}{Y_P} T_1 + d_{31} E_3, \\ D_3 &= d_{31} T_1 + \varepsilon_{33} E_3, \end{aligned} \tag{9}$$

where S_1 is the scalar strain, Y_P is Young's modulus for the piezoelectric material, T_1 is the scalar stress, d_{31} is a material constant, E_3 is the electric field, D_3 the electric displacement, and ε_{33} the permittivity of the piezoelectric material.

The modes of vibration that cause chatter are essentially the bending modes of the tool and spindle structure. The region of the tool where the piezoelectric material is mounted can therefore be treated as a beam structure such as that shown in Fig. 8, although in practice the beam cross-section is cylindrical rather than rectangular. Ignoring the electromechanical coupling of the piezoelectric material, the measured voltage as a function of time, $v_s(t)$, can be written as [17]

$$\begin{aligned} v_s(t) &= k_s(y'(t, x_2) - y'(t, x_1)), \\ k_s &= \frac{Y_p d_{31} b_p \left(t_b + t_p/2\right)}{C_p}, \end{aligned} \tag{10}$$

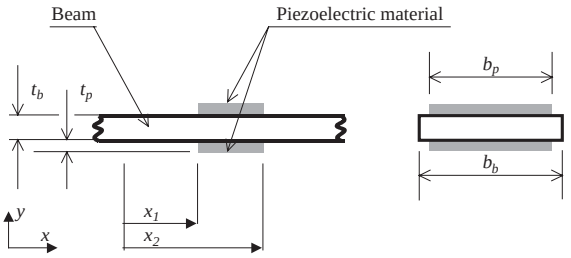

Fig. 8. Beam geometry and nomenclature.

where x_1 is the position of the start of the piezoelectric material along the axis of the beam, and x_2 the end. The coordinate y is the deflection of the beam, b_p is the breadth of the piezoelectric material, t_p its thickness, and t_b the beam thickness. C_p is the capacitance of the piezoelectric device, and k_s is the sensor gain.

For a non-sensing actuator on the same beam structure, the actuator produces a bending moment M_a as a function of time t and position x on the beam, which (again ignoring electromechanical coupling) can be written as [17]

$$\begin{aligned} M_a(t,x) &= k_a v_a(t)[h(x-x_1)-h(x-x_2)], \\ k_a &= b_b d_{31} Y_p\left(t_p + t_b\right), \end{aligned} \tag{11}$$

where k_a is the actuator gain, v_a is the actuator voltage and $h(x)$ is the Heaviside step function.

A detailed investigation of piezoelectric actuators was described by Crawley and de Luis [15]. It was shown that surface-bonded actuators with perfect bonds apply concentrated moments at their edges, as shown in Eq. (11), whilst for imperfect bonds the shear transfer from actuator to host material results in a distributed moment.

In the foregoing analysis, the electromechanical coupling of the piezoelectric material has been ignored. In practice, the coupling can have the effect of changing the stiffness of the structure [18,19]. For example, Preumont [19] describes the finite element formulation of a shell structure with surface-mounted piezoelectric material [20]. It was shown that in the 'open circuit' condition, the usual mass and stiffness matrices are modified to become

$$M_{xx}\ddot{x} + \left(K_{xx} - K_{x\varphi}K_{\varphi\varphi}^{-1}K_{\varphi x}\right)x = f, \tag{12a}$$

whereas when the piezoelectric material is driven by a voltage, the system equations are

$$M_{xx}\ddot{x} + K_{xx}x = f - K_{x\varphi}\varphi, \tag{12b}$$

where f is the applied mechanical load, M_{xx} is the mass matrix, K_{xx} the stiffness matrix, $K_{\varphi\varphi}$ the electrical capacitance, and x the resulting displacements. $K_{x\varphi}$ and $K_{\varphi x}$ are coupling matrices between the mechanical and electrical loads, and vice versa. Even without a detailed analysis of this result it is apparent that, depending upon the electrical connection of the piezoelectric material, the electromechanical coupling can modify the effective stiffness of the system.

2.2.3. Modal analysis

In the case of non-piezostructures, the modal analysis approach is well known and a summary is given here based upon the methods used in Ref. [21]. Given the experimental receptance frequency response data for a continuous system from an excitation at actuator location 2 to a response at sensor location 1, $H_{12}(\omega)$, and assuming that each mode has proportional viscous damping, the response can be written as [22]

$$H_{12}(\omega) = \sum_{n=1}^{\infty} \frac{\phi_{1n}\phi_{2n}}{\omega_n^2 + 2\mathrm{j}\omega\varsigma_n\omega_n - \omega^2}, \tag{13}$$

where ϕ_{1n} is the mode shape for the nth mode of vibration at the sensor location, and ϕ_{2n} is the mode shape for the nth mode of vibration at the actuator location. A modal model based upon the first M modes of vibration is

$$a_{12}(\omega) = \sum_{n=1}^{M} \frac{{}_nA_{12}}{\omega_n^2 + 2\mathrm{j}\omega\varsigma_n\omega_n - \omega^2} + E_{0,12}, \tag{14}$$

where $E_{0,12}$ represents the contributions of the truncated nodes as a static correction. The modal constants (${}_nA_{12}$), natural frequencies (ω_n), and damping ratios (ζ_n) can be identified using a number of methods such as the peak-picking method, the circle fit method, or nonlinear least-squares algorithms [23]. The modal constant ${}_nA_{12}$ is related to the mode shapes by

$${}_nA_{12} = \phi_{1n}\phi_{2n}, \tag{15}$$

Modal analysis methods have been applied to piezostructures by a number of researchers, but in general the aim has been to predict mode shapes and natural frequencies rather than to predict a properly scaled frequency response function. For example, Cole et al. [24] considered piezoelectric sensors, actuators, and sensoriactuators as coupled electromechanical devices, and showed that the modal model can include mode shapes for the sensors and actuators. Hagood et al. [25] and Kanawa [26] also investigated piezostructure dynamics, although their analysis was from a control perspective.

Wang [27,28] and co-workers assumed constant actuator and sensor gains, similar to those used by Dosch [17], and showed that the analytical mode shapes for beams with surface-mounted actuators or sensors can be rewritten as the difference between the mode shape slopes at the two edges of the transducer:

$$\phi_{pn} = \phi'_n(x_2) - \phi'_n(x_1), \tag{16}$$

where the subscript p denotes the piezoelectric material location, and n is the mode of vibration. The coordinates x_1 and x_2 are as for Eqs. (10) and (11), and ϕ is the derivative of the deflection mode shape with respect to x. More recently, this theoretical work has been applied to laboratory vibration problems [29]. The relevance of Eq. (16) to the present study is that it demonstrates that the FRFs for piezoelectric sensors and actuators can still be represented by modal models, and that a piezoelectric sensor will have the same mode shape as a piezoelectric actuator in the same location.

Returning to Eq. (14) and Fig. 7b, the nth mode shape at the piezoelectric sensor/actuator is defined as ϕ_{pn}, and the nth mode shape at the tip of the tool is defined as ϕ_{tn}. The modal model

is now:

$$\alpha_{pp}(\omega) = \frac{1}{k_a k_s}\frac{v_s(\omega)}{v_a(\omega)} = \sum_{n=1}^{M} \frac{{}_nA_{pp}}{\omega_n^2 + 2\mathrm{j}\omega\varsigma_n\omega_n - \omega^2} + E_{0,pp} \tag{17}$$

$$\alpha_{tp}(\omega) = \frac{1}{k_a}\frac{x(\omega)}{v_a(\omega)} = \sum_{n=1}^{M} \frac{{}_nA_{tp}}{\omega_n^2 + 2\mathrm{j}\omega\varsigma_n\omega_n - \omega^2} + E_{0,tp} \tag{18}$$

where the modal constants ${}_nA_{pp}$ and ${}_nA_{tp}$ can be identified. This leads to the mode shapes of the co-located piezoelectric sensor and actuator:

$$\phi_{pn} = \sqrt{{}_nA_{pp}}, \tag{19}$$

which can be used to find the mode shape at the tip of the tool:

$$\phi_{tn} = \frac{{}_nA_{tp}}{\phi_{pn}}, \tag{20}$$

from which the response at the tip of the tool can be predicted:

$$\alpha_{tt}(\omega) = \frac{x_t(\omega)}{F_t(\omega)} = \sum_{n=1}^{M} \frac{\phi_{tn}\phi_{tn}}{\omega_n^2 + 2\mathrm{j}\omega\varsigma_n\omega_n - \omega^2} + E_{0,tt}, \tag{21}$$

which is equivalent to the term $G(\omega)$ using in the preceding analysis of chatter stability. However, the residual term, $E_{0,tt}$, is unknown and so the predicted response can only include the modes that were included in the modal model. This prediction is denoted by the superscript ^{P}, giving

$$\alpha_{tt}^P(\omega) = \sum_{n=1}^{M} \frac{\phi_{tn}\phi_{tn}}{\omega_n^2 + 2\mathrm{j}\omega\varsigma_n\omega_n - \omega^2} \approx \frac{x_t(\omega)}{F_t(\omega)}. \tag{22}$$

Near the resonant frequencies the response is dominated by the corresponding mode of vibration, so the residual $E_{0,tt}$ will be negligible and Eq. (22) will be accurate. Near the antiresonances, the residual term will have a significant effect and so Eq. (22) will be less accurate. Fortunately, from the point of view of stability lobes, we are often only interested in the real part of the response when it is negative and of high magnitude, and so the antiresonances are not so important.

2.2.4. Application

To summarise, there has been a great deal of research that has attempted to characterise the performance of surface-mounted piezoelectric sensors and actuators. The majority of this work has assumed that the host structure is a beam or shell. In the case of a milling tool, regenerative chatter is usually a result of the bending modes of the tool/spindle structure, and so these assumptions remain valid. Piezoelectric materials exhibit electromechanical coupling which (as with many previous studies) has been neglected here, although in practice this coupling can act to modify the stiffness of the structure.

One potential pitfall with the use of surface-bonded piezoelectric devices is the accuracy of the sensor and actuator gains (Eqs. (10) and (11)). For some modal testing scenarios using

piezoelectric devices, the practitioner may only be interested in determining the natural frequencies and unscaled mode shapes, in which case the transducer gains are not important. However, from the point of view of stability lobe prediction, the desired FRF will be scaled by both of the transducer gains. Errors in the gains could be caused by a number of factors, such as: day to day changes in the piezoelectric capacitance, inaccuracy of the piezo/host geometry, and the validity of the assumptions behind Eqs. (10) and (11). The latter two examples are more likely to occur on tools where the flat piezo-transducer will be bonded to a cylindrical surface, resulting in thick, irregular glue lines. Furthermore, it has been shown by considering the electrical equivalent circuit of the electromechanically coupled piezostructure [26] that the sensor/actuator gain is a function of the sensor/actuator placement. It is therefore desirable to develop a practical method for calibrating the transducer gains.

In the case where the piezoelectric sensor and actuator gains, k_s and k_a, are subject to error factors, the prediction of α_{tt}^P will be scaled accordingly. With reference to Eq. (21), it is well known [23] that the static stiffness at location t due to a load at location t should match the prediction α_{tt} at zero frequency. Assuming the residual term ($E_{0,tt}$) is negligible, the prediction α_{tt}^P can be scaled by a factor K so that its zero-frequency value matches the static deflection of the structure. This will correct for the calibration errors of the sensor and actuator.

3. Numerical study

Section 2 has demonstrated that the prediction of tool stability lobes using piezo transducers draws on theory from three main areas: machine dynamics, modal analysis, and smart structures. An alternative approach has been proposed for predicting the required FRF based upon a modal model. In addition, a static calibration procedure has been described to account for variations in the sensor and actuator gains.

To begin, these concepts were explored numerically using a finite element model of a cantilever beam—so-called 'synthetic modal analysis'. It should be noted that this structure is not intended to resemble a milling tool, but to assess the modal model and static correction approach on a simple structure. The model geometry is summarised in Table 1, and the piezoelectric actuation was modelled as two discrete bending moments (of opposite sign) corresponding to the edges of the piezoelectric actuator. The piezoelectric sensor was modelled as the 2 rotational degrees of freedom at the same locations, and scaling errors were then introduced into the sensor and

Table 1
Geometry of the FE model

Material properties	As steel
Beam thickness, t_b (mm)	3
Beam width, b_b (mm)	19
Distance of piezoelectric material from built-in end (mm)	30
Length of piezoelectric material (mm)	19
Length of beam (mm)	130

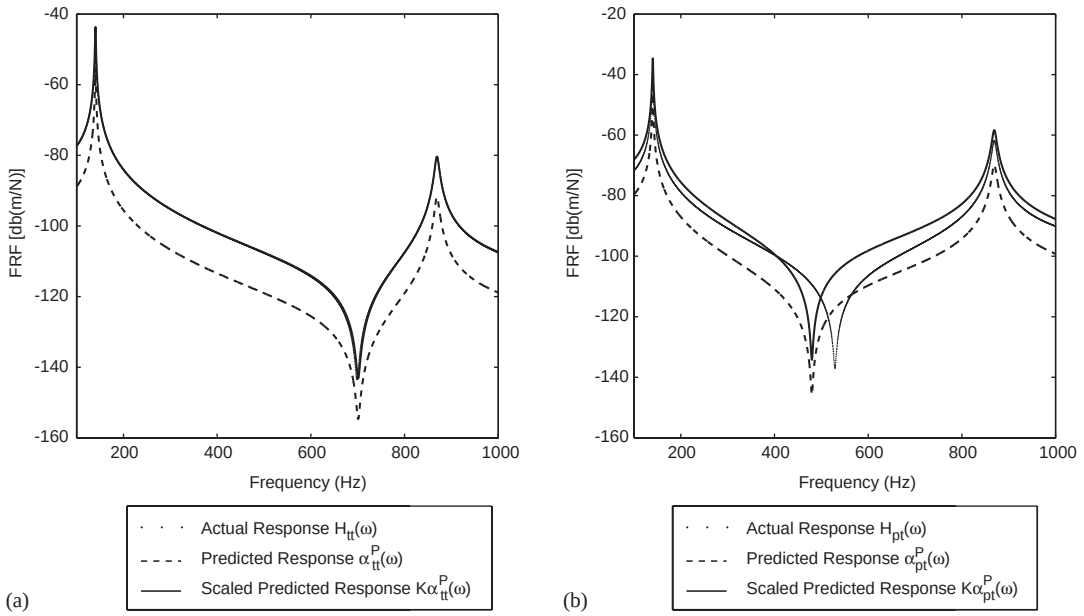

Fig. 9. Numerical results from an FE model of a cantilever beam. (a) Comparison between driving-point FRF and the FRF predicted from the response to piezoelectric actuation. (b) Comparison between the true response of the piezoelectric sensor to direct excitation at the tip, and the sensor response predicted from the beam's behaviour during piezoelectric actuation.

actuator responses. A modal model was generated based upon this data, and the model used to predict the response at the tip of the beam. This predicted response was then scaled so that its dc value matched the static deflection stiffness at the top of the beam.

The driving-point frequency response at the free end of the beam was determined and compared to the predicted result.

In Fig. 9, the modal model prediction is compared to the FE model response for the driving-point FRF at the tip of the beam. It can be seen that, after recalibrating the response by matching the static deflection to that from the FE model, the predicted driving-point FRF at the tip is virtually identical to the actual driving-point FRF at the tip. For the predicted response at the piezoelectric sensor, there is some difference, particularly in the antiresonance frequency. This is due to the absence of a residual term for the truncated modes, this term having a much larger effect for the piezoelectric mode shape than for the tip mode shape.

It has therefore been shown that the proposed method is valid either near the modelled natural frequencies, or when the unknown static correction term, $E_{0,tt}$, is small.

4. Experimental study

A milling tool was then tested in the laboratory. The tool was rigidly clamped using a lathe chuck fastened to a rigid foundation, and piezoelectric surface patches added near the root of the

Table 2
Geometry and properties of the milling tools with surface-mounted piezoelectric material

Type	Carbide end mill
Diameter (“)	0.375
Free length (“)	2.25
t_p (mm)	0.191
b_p (mm)	10
Distance or piezoelectric material from root of tool (mm)	4
Piezoelectric material length (mm)	8
No. flutes	2
Manufacturer	Robb Jack Corporation
Adhesive	Loctite E-00NS
Piezoelectric material	Piezo Systems PSI-5A4E

tool using an epoxy adhesive. The geometry of the tool is described in Table 2. The tool was excited using a chirp voltage passing through a voltage amplifier to the piezoelectric actuator.

The deflection at the tool tip was measured using an accelerometer, and the piezoelectric sensor voltage was measured directly. SigLab signal-processing hardware was used to estimate the corresponding frequency response functions, and these were then processed using the Matlab Structural Dynamics Toolbox, to predict the FRF at the tip of the tool, α_{tt}^{P}.

A dead-weight test was then performed by hanging a small weight off the end of the tool and measuring the resulting deflection with a capacitance probe. The resulting value of static stiffness was used to created the calibrated response prediction, $K\alpha_{tt}^{P}$.

For comparison purposes, a small modal hammer was used to excite the tool tip at the same location as the accelerometer, and the driving-point FRF, H_{tt}, estimated.

The analytical stability lobes were then generated by assuming that the orientated transfer function, G_{OTF}, is equal to the measured (H_{tt}) or predicted ($K\alpha_{tt}^{P}$) frequency response function. For comparison purposes this assumption makes no difference, although in practice it is equivalent to a slot milling operation using a tool with equal FRFs in the directions normal and parallel to the workpiece feed direction.

The tool tested was observed to have two bending modes occurring below 5 kHz, along with a mode at around 2.6 kHz. Modal models were created with just the two main bending modes, and all three modes. Fig. 10 shows the real-FRF predictions in the region of each natural frequency. There are small differences in the natural frequency and magnitude when compared to the actual response. However, Fig. 11 shows that these errors have little effect on the stability lobes for the tool: there is excellent agreement between the predicted lobes and those obtained with the modal hammer. Including the mode at 2.6 kHz (Fig. 10b) enables the most accurate prediction of the stability lobe.

Fig. 12 attempts to investigate the effect of the piezoelectric transducers on the stability lobes for this tool, by testing the tool (with a modal hammer) before and after the addition of the transducer patches. The lobes remain largely unaffected by the addition of the patches, but since the tool was removed from its holder between the two tests, the repeatability of this result is questionable and further work is required to properly assess the influence of small piezoelectric patches on the stability lobe plot.

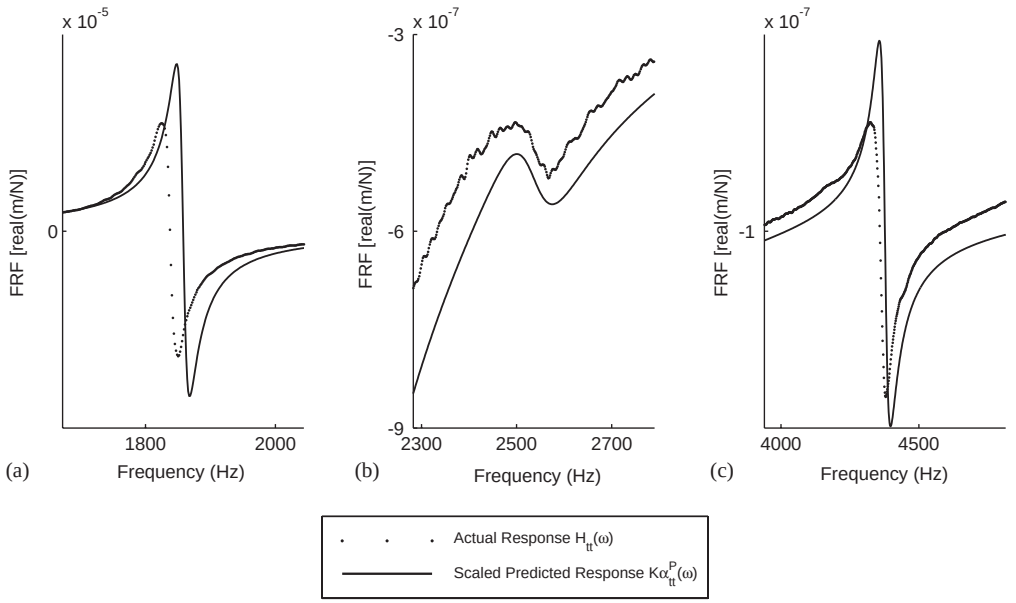

Fig. 10. Tool TIP FRFs (displacement/force) obtained (1) by direct impact with a modal hammer and (2) predicted from the response of the tool to piezoelectric actuation. (a) Mode 1; (b) mode 2; (c) mode 3.

5. Discussion

The results described in the previous section have demonstrated the validity of the proposed method. However, a number of points are worthy of further discussion:

First, the configuration of the piezoelectric patches (as shown in Fig. 8) means that the piezoelectric actuator and sensor are not truly collocated, which could lead to errors in the modal analysis. If further work demonstrated that these errors were significant, sensoriactuators [17,30,31] could be used to ensure collocality. However, this approach may be more sensitive to electrical interference, and would need additional hardware.

A second issue arising from the configuration of the piezoelectric patches is that extension and torsion modes of vibration may be excited, as well as bending modes. Extension modes would not be excited if a pair of actuators were used, placed on opposite sides of the structure, and working in opposing directions. This would induce pure bending but would require a sensoriactuator configuration to enable a collocated measurement. Torsion modes would be excited if the patches are not square and parallel when bonded to the surface. However, it may be that these modes (extensional and torsional) are also capable of producing chatter. In this case, the ability to excite these modes would be a distinct advantage compared to the traditional approach using a modal hammer.

A further consideration is that the piezoelectric transducers must be sufficiently small to properly excite or measure the mode of vibration.

The use of a static calibration to scale the FRF predictions could cause problems since this measurement becomes more difficult on small tools and may be difficult to implement within a machine structure. However, it is possible that the calibration process could be carried out before testing in the machine.

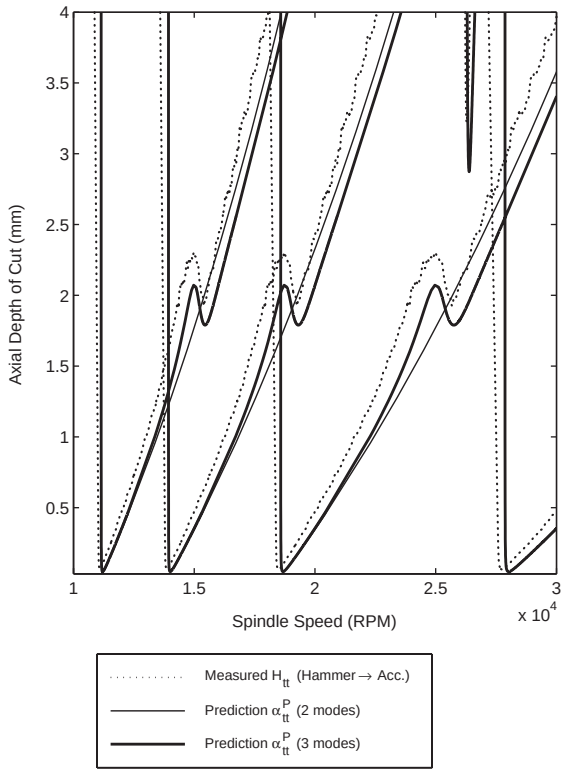

Fig. 11. Stability lobes for the tool obtained (1) by direct impact using a modal hammer at the tool tip and (2) predicted from the response of the tool to piezoelectric actuation.

It should be noted that the tools tested in this study were rigidly clamped, and further work is needed to test tools that are held on a milling machine spindle. However, the modal models generated from a rigidly clamped tool could be combined with data from a machine spindle using a substructure analysis technique [3]. Alternatively, a slip ring assembly or telemetry system could be used so that the electrical connections shown in Fig. 7a and b can be achieved during operation of the machine.

A final issue that is worth mentioning is the validity of the test data from the modal hammer. As mentioned in Section 1, this method requires an experienced user and is itself dependent upon accurate calibration of the force sensor across the frequency range. Consequently, it can be argued that the differences seen in the results presented here are actually due to errors in measurements with the modal hammer, rather than errors in the predictions with piezoelectric devices.

6. Conclusions

A new modal test procedure has been described for the prediction of milling tool stability lobes, using surface-mounted piezoelectric transducers. The approach relies on the assumption that the

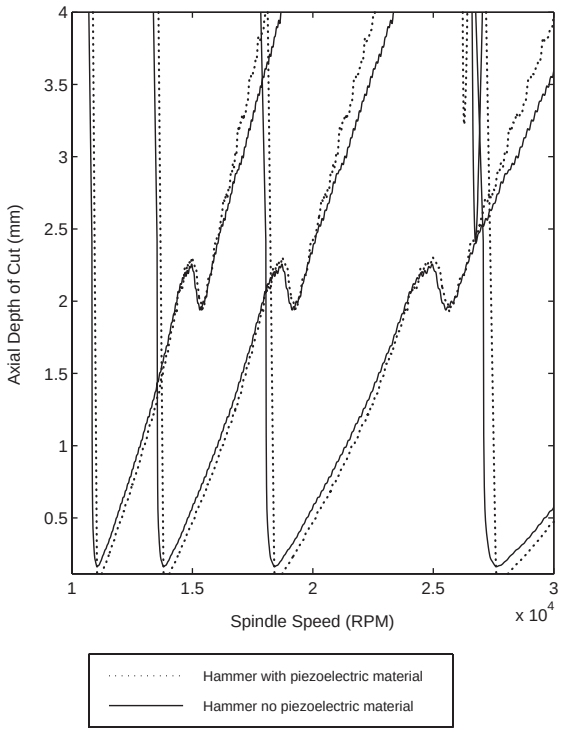

Fig. 12. Stability lobes using modal hammer FRFs before and after the piezoelectric transducers were glued on.

static correction (introduced by a truncaton of the modal model) is negligible. This assumption has been shown to be valid for both numerical studies based upon cantilever beams, and on milling tools tested in the laboratory.

The experimental tests have demonstrated good agreement with traditional stability test procedures which rely on a modal hammer, and the new method is particularly well suited to use on small milling tools which can be difficult to test with a modal hammer. It is suggested that the proposed technique could be used for automated chatter testing using intelligent tools with embedded piezoelectric transducers.

Finally, the proposed technique may prove useful to other applications of vibration testing where a frequency response function is to be predicted at a sensor location, when the system is excited by surface-mounted piezoelectric actuators.

Acknowledgements

The authors are grateful for the support of the EPSRC (grant R63806), and the Advanced Manufacturing Research Centre, with The Boeing Company, at The University of Sheffield.

References

[1] J. Tlusty, M. Polacek, The stability of the machine tool against self excited vibration in machining, in: *ASME Proceedings of the Engineering Research Conference*, Pittsburgh, PA, 1963.

[2] TXF, Manufacturing Laboratories, Inc., 2002.

[3] T. Schmitz, M. Davies, M. Kennedy, Tool point frequency response prediction for high-speed machining by RCSA, *Journal of Manufacturing Science and Engineering* 123 (2002) 1–8.

[4] SPA, Manufacturing Laboratories, Inc., 2002.

[5] T. Delio, J. Tlusty, S. Smith, Use of audio signals for chatter detection and control, *Transactions of the ASME* 114 (1992) 146–157.

[6] S. Smith, W.R. Winfough, The effect of runout filtering on the identification of chatter in the audio spectrum of milling, *Transactions of the NAMRI/SME* 22 (1994) 173–178.

[7] J.P. Snyder, M. Davies, J. Pratt, S. Smith, A new stable speed test apparatus for milling, *Transactions of the NAMRI/SME* 24 (2001) 153–157.

[8] J. Tlusty, *Manufacturing Processes and Equipment*, Prentice-Hall, Englewood Cliffs, NJ, 1999.

[9] S. Smith, J. Tlusty, An overview of modeling and simulation of the milling process, *Journal of Engineering for Industry* 113 (1991) 169–175.

[10] S. Smith, J. Tlusty, Update on high-speed milling dynamics, *Transactions of the ASME* 112 (1990) 142–149.

[11] M. Wiercigroch, E. Budak, Sources of nonlinearities chatter generation and suppression in metal cutting, *Philosophical Transactions of the Royal Society of London Part A* 359 (2001) 663–693.

[12] Y. Altintas, D. Montgomery, E. Budak, Dynamic peripheral milling of flexible structures, *Journal of Engineering for Industry* 114 (1992) 137–145.

[13] Y. Altintas, E. Budak, Analytical prediction of stability lobes in milling, *CIRP Annals* 44 (1995) 357–362.

[14] T. Delio, TXF, Manufacturing Laboratories, Inc., 2002.

[15] E.F. Crawley, J. DeLuis, Use Of piezoelectric actuators as elements of intelligent structures, *AIAA Journal* 25 (10) (1987) 1373–1385.

[16] Y. Kawaga, G.M.L. Gladwell, Finite element analysis of flexure-type vibrations with electrostrictive transducers, *IEEE Transactions on Sonics and Ultrasonics* 17 (1970) 41–49.

[17] J.J. Dosch, D.J. Inman, E. Garcia, A self-sensing piezoelectric actuator for collocated control, *Journal of Intelligent Material Systems and Structures* 3 (1992) 166–185.

[18] S.M. Yang, Y.J. Lee, Modal analysis of stepped beams with piezoelectric materials, *Journal of Sound and Vibration* 176 (1994) 289–300.

[19] A. Preumont, *Vibration Control of Active Structures*, Dordrecht, Kluwer, 2002.

[20] H. Allik, T.R.J. Hughes, Finite element method for piezoelectric vibration, *International Journal of Numerical Methods in Engineering* 2 (1970) 151–157.

[21] E. Balmès, Structural Dynamics Toolbox, 2002.

[22] E. Balmès, Frequency domain identification of structural dynamics using the pole/residue parametrization, in: *International Modal Analysis Conference*, 1996.

[23] D.J. Ewins, *Modal Testing: Theory Practice and Application*, Research Studies Press, Letchwer, 2000.

[24] D.G. Cole, S.W. Re, H.H. Robertshaw, Modal parameter estimation for piezostructures, *Journal of Vibration and Acoustics* 117 (1995) 431–438.

[25] N.W. Hagood, W.H. Chung, A.V. Flotow, Modelling of piezoelectric actuator dynamics for structural control, *Journal of Intelligent Material Systems and Structures* 1 (3) (1990) 327–354.

[26] Y. Kawaga, T. Tsuchiya, N. Wakatsuki, Equivalent circuit representation of a vibrating structure with piezoelectric transducers and the stability consideration in active damping control, *Smart Materials and Structures* 10 (2001) 389–394.

[27] B.-T. Wang, C.-C. Wang, Feasibility analysis of using peizoceramic transducers for cantilever beam modal testing, *Smart Materials and Structures* 6 (1997) 106–116.

[28] B.-T. Wang, Characterization of transfer functions for piezoceramic and conventional transducers, *Journal of Intelligent Material Systems and Structures* 7 (1996) 390–398.

[29] B.-T. Wang, R.-L. Chen, The use of piezoceramic transducers for smart structural testing, *Journal of Intelligent Material Systems and Structures* 11 (9) (2000) 713–724.
[30] D.G. Cole, R.L. Clark, Adaptive compensation of piezoelectric sensoriactuators, *Journal of Intelligent Material Systems and Structures* 5 (1994) 665–672.
[31] J.S. Vipperman, R.L. Clark, Hybrid analog and digital adaptive compensation of piezoelectric sensoriactuators, in: *AIAA/ASME/ASCE/AHS Structures, Structural Dynamics & Materials Conference*, AIAA, New Orleans, LA, USA, 1995.